Cut-n-Reveal: Time Series Segmentations with Explanations

NIKHIL MURALIDHAR and ANIKA TABASSUM, Virginia Tech
LIANGZHE CHEN, Pinterest
SUPRIYA CHINTHAVALI, Oak Ridge National Laboratory
NAREN RAMAKRISHNAN, Virginia Tech
B. ADITYA PRAKASH, Georgia Institute of Technology

Recent hurricane events have caused unprecedented amounts of damage on critical infrastructure systems and have severely threatened our public safety and economic health. The most observable (and severe) impact of these hurricanes is the loss of electric power in many regions, which causes breakdowns in essential public services. Understanding power outages and how they evolve during a hurricane provides insights on how to reduce outages in the future, and how to improve the robustness of the underlying critical infrastructure systems. In this article, we propose a novel scalable segmentation with explanations framework to help experts understand such datasets. Our method, CnR (Cut-n-Reveal), first finds a segmentation of the outage sequences based on the temporal variations of the power outage failure process so as to capture major pattern changes. This temporal segmentation procedure is capable of accounting for both the spatial and temporal correlations of the underlying power outage process. We then propose a novel explanation optimization formulation to find an intuitive explanation of the segmentation such that the explanation highlights the *culprit* time series of the change in each segment. Through extensive experiments, we show that our method consistently outperforms competitors in multiple real datasets with ground truth. We further study real county-level power outage data from several recent hurricanes (Matthew, Harvey, Irma) and show that CnR recovers important, non-trivial, and actionable patterns for domain experts, whereas baselines typically do not give meaningful results.

CCS Concepts: • **Networks** → *Sensor networks*; • **Information systems** → **Data mining**; **Spatial-temporal systems**;

Additional Key Words and Phrases: Multivariate time series, spatio-temporal segmentation

1   INTRODUCTION

Power outages during several recent hurricanes have had a severe impact on our national security,
economy, and public safety. The 2017 hurricane season was the most expensive in U.S. history,
resulting in huge economic losses (greater than $250 billion). Hurricane Irma caused one of the
largest power outages, which reportedly knocked out power to 4.5 million of the 4.9 million Florida
Power & Light customers. Hence, better understanding of power outages and how they evolve
during hurricanes is a very important task for damage prevention and control.

Domain experts in critical infrastructure systems (CIS) constantly seek solutions and ideas on
how to reduce power outages during hurricanes. For example, the Oak Ridge National Laboratory
(ORNL) Energy Awareness and Resiliency Standardized Services (EARSS) project developed a fully
automated procedure to take wind speed and location estimates provided by hurricane monitoring
experts and provide a geo-spatial estimate on the impact to the electric grid in terms of outage areas
and projected duration of outages [12].

Retrospectively identifying "cut-points" with a sudden change in the number of outages in
historical data can help in many aspects, such as identifying phases and causes through inter-
dependency analysis. This helps disaster management personnel learn from past events and be
better prepared for future contingencies. For example, a retrospective analysis of Hurricane Sandy
highlighted the underlying causes due to inter-dependencies with communication, oil, and natural
gas infrastructures [8]. Further, pinpointing "culprit" counties responsible for each such cut-point
helps domain experts localize points of failure and analyze restorative periods [21]. Hence, such
analysis can be used to shorten restoration periods of vulnerable points in the grid, thereby im-
proving grid resiliency to future disasters.

The preceding analysis goals may be addressed using the time series mining task of "segmen-
tation." However, computing interpretable "culprits" for each cut-point is a task that has not been
studied before. In this article, we address this issue via a novel segmentation-with-explanations
approach. Our main contributions are the following:

- We propose a novel problem and algorithm CnR (Cut-n-Reveal) for computing segments
  of power outage data. CnR captures temporal and spatial relationships between counties
  experiencing power outages, modeling the power failure process as a segmentation problem
  (see Figure 1). We also propose a novel explanation algorithm that identifies the *culprit*
  counties for each segmentation cut-point.
- Our proposed formulation uses low-dimensional latent factor models and achieves signifi-
  cant speedup.
- Experiments were performed with CnR and other popular segmentation algorithms on syn-
  thetic and real datasets including historical hurricane power outage data. The other segmen-
  tation procedures perform significantly worse relative to CnR on the real hurricane data,
  due to their inability to model complex spatial dynamics of the failure process. Although
  CnR is developed for power outage data, it can be applied to any multivariate time series.

The rest of the article is organized as follows. In Section 2, we formally state the segmen-
tation and explanation problems. Section 3 introduces our spatially agnostic CnR-V (Temporal

(a) Temporal segmentation to identify different failure phases of the power grid across all counties affected by Hurricane Matthew.

(b) Spatial clustering revealed by CnR of counties in Florida that experienced extensive damage (in green) to power infrastructure due to Hurricane Matthew.
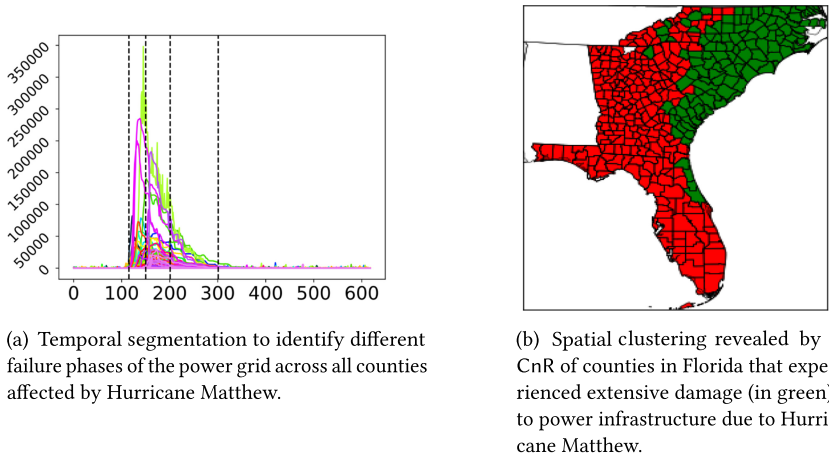
Fig. 1. An example of the holistic spatial and temporal analysis results from our novel CnR model to analyze the damage to the power grid during Hurricane Matthew. (a) The overall temporal segmentation over a dataset where each time series indicates the total number of households that lost power in a single county over the course of Hurricane Matthew (household count per county is recorded every hour). (b) The spatial clustering of all counties that experienced significant damage to power infrastructure through the course of Hurricane Matthew, essentially representing the spatial span of damage.

Cut-n-Reveal) segmentation and explanation model. We then introduce the novel spatio-temporal CnR-UV (Spatio-temporal Cut-n-Reveal) model in Section 4, designed to incorporate extensive spatial information for segmenting and explaining failure process dynamics in a multivariate time series. Section 5 showcases the performance of CnR-UV with respect to other state-of-the-art algorithms and on real-world problems. Section 6 provides a brief review of related literature, and Section 7 explores avenues for future work. For lack of space, we defer some additional experiments to the appendix [6]. All codes and datasets are made public [7].

2 FOCUS AND SETUP

Motivation. Large power grids usually contain thousands of generators, hundreds of thousands of transmission lines, and millions of consumers. Grid components have strong inter-dependencies, such as in the transmission grid where multiple paths exist between generators and consumers, and these paths typically are arranged in a mesh grid manner. Hence, if one path or line fails, the electricity instantaneously follows an alternate path governed by Kirchhoff's voltage and current laws. If the alternate path, however, cannot handle the overload in flow, it in turn fails and this failure cascades to neighboring components. Due to the well-studied property of cascading failures and small-world properties in the power grid [26, 28], a few initial points of failure due to a hurricane quickly cause network instability in a region, potentially causing millions of people to suffer the effects of brownouts or blackouts. Natural disasters like hurricanes exhibit multiple phases of varied intensity along their path, causing failures with different levels of severity at different regions. We model the progression of this grid failure process as a temporal segmentation problem. Modeling this failure process over time, across different regions (e.g., counties) affected by a hurricane, is essential for improving the resilience of critical infrastructure to disasters.

Focus. We characterize the severity of this grid failure process by measuring the number of people in a hurricane-affected region (a county in our case) without power over the entire time

period of the hurricane. Three critical questions need to be answered for characterization of this process:

- How can we identify different phases of a hurricane as a function of severity of the damage to critical infrastructure like the power grid, using sparse customer power loss data?
- Which counties are most important for characterizing each phase?
- How can counties be grouped together based on their overall failure dynamics during the hurricane?

Our main goal is to help domain experts answer the aforementioned questions.

Notation. We assume that we are given a set of time series $X = \{x_1, x_2, \ldots, x_n\}$, where each time series $x_i = [x_i(t_1), x_i(t_2), \ldots, x_i(t_m)]$, and $x_i(t_j)$ represents the value at timestamp t_j for the ith time series. We also assume that there is a known underlying graph structure G that captures the relationship among these time series $\{x_i\}$. For example, in CIS, the number of electric outages in all disaster-affected counties form a set of time series, and the relationship among these counties can be based on their geographical proximity.

Definitions. Our algorithm CnR contains two parts: detecting a good *segmentation* of the outage data to capture the main changes and finding the corresponding *explanations* (subset of important counties) per segment. With this knowledge of the segmentation and the explanations for each segment, the expert has a holistic picture of the different phases of the failure process, as well as the specific time series that contributed significantly to each phase change. We now formally state our definition of a segmentation and an explanation.

Definition 1 (Segmentation S). A segmentation of X contains a set of distinct temporal cut-points $S = \{c_1, c_2, \ldots, c_k\}$, where $c_i \in \{t_1, t_2, \ldots, t_m\}$.

Definition 2 (Explanations E). $E = \{e_1, e_2, \ldots, e_k\}$, where e_i is an n by 1 non-negative explanation vector. $||e_i||_1 = 1$, and e_{ij} represents the importance of time series j for explaining the cut-point c_i.

Setup. The cut-points of S naturally divide the entire time period in the dataset into a set of disjoint time segments. The ith time segment is denoted as a set of contiguous timesteps $s_i = [c_{i-1}, c_i)$ with $i \in \{1, 2, \ldots, k+1\}$, $c_0 = t_1$, and $c_{k+1} = t_m$. Two sets/segments s_i, s_j are said to be neighboring segments if $s_i = \{t_l, \ldots, t_{l+\Delta l}\}$ and s_j contains t_{l-1} or $t_{l+\Delta l+1}$.

Assuming that we are given a segmentation S of X, containing a set of cut-points $\{c_i\}$ and corresponding segments, $\{s_i\}$, a desired explanation of the segmentation should be simple yet effective enough to guide efforts to prevent or curtail the effects of critical infrastructure failure in future disasters.

To this end, we introduce an explanation vector e_i for each cut-point c_i in S. Each e_i is an $n \times 1$ vector, where n represents the number of counties and e_{ij} represents the importance of the jth time series/county in explaining the cut-point. Intuitively, if time series x_j shows very different patterns before and after the cut-point c_i, we consider it important in explaining why c_i is a good cut-point. However, if x_j remains constant/unchanged across c_i, it does not provide useful information in terms of the cut-point c_i and should have low values in e_i. In the hurricane outage data where there are hundreds of time series/counties, such explanation vectors are able to highlight the "culprit" time series/counties.

We propose two versions of the CnR algorithm, namely CnR-V and CnR-UV. Sections 3.1 and 3.2 discuss the segmentation and explanation formulations and corresponding solutions using CnR-V. Sections 4.1 and 4.2 detail our segmentation and explanation solutions using CnR-UV.

3 TEMPORAL CUT-N-REVEAL

In this section, we propose our CnR-V model, which performs segmentation on a multivariate time series only using temporal information and also yields explanations for each segmentation cut-point.

3.1 CnR-V Segmentation

The segmentation problem addressed by CnR-V is stated as follows.

PROBLEM 1. *Given a set of time series X and a number k, find the k-segmentation of S that captures the main pattern changes in X.*

3.1.1 Overview of Our Approach. Through the segmentation model, we wish to isolate temporal sequences into discrete segments such that the properties of the failure process in each segment differ from neighboring segments. The process of manually or algorithmically picking reasonable segments is non-trivial, as segments that are too small fail to capture significant properties of the failure process and picking segments that are too large although capturing all failure process characteristics do not highlight the differences between the various phases of the process. Since the failure process is highly dynamic and the failure dataset is sparse in nature, methods based on capturing long-term correlation [25] or invariant learning [37] from the data will be unable to perform adequately.

3.1.2 Formulation. We consider the different phases of the failure process in the power grid during natural disasters as a collection of disjoint segments $\{s_1, \ldots, s_{k+1}\}$. We wish to discover a collection of k cut-points S that minimizes similarity between any two neighboring segments s_i, s_j. Hence, each segment s_i would capture a different pattern from its neighboring segments (s_{i-1}, s_{i+1}), and thus the segmentation S captures pattern changes in the time series. We employ the normalized cut framework, which has been shown to work well in subspace clustering and segmentation tasks [50]. Our goal now is to represent each timestep by allowing for effective similarity calculation between timesteps so that the continuous evolution of the failure process is captured by the inter-timestep similarity. In an effort to find a principled approach to capture the similarity between different timesteps in the failure process, we adopt the formulation provided by Tierney et al. [52] for video scene segmentation for our purposes of modeling the hurricane failure process. The model represents each timestep in the data X, as a function of other important timesteps. It is through this latent representation V that we attempt to capture the dynamics in the data X.

$$\min_V \frac{1}{2}||X - XV||_F^2 + \lambda_1||V||_1 + \lambda_2||VR||_{1,2}$$
$$\text{subject to} \quad \textbf{diag}(V) = 0$$

(1)

In Equation (1), V is an m by m matrix whose i^{th} column can be considered the latent representation of timestep i in terms of all other timesteps. The first term in Equation (1) calculates the reconstruction error between X and XV, whereas the second term introduces sparsity into the latent representation, enforcing that each timestep be explained as a function of a small subset of other important timesteps. The term VR (R is defined in Table 1) calculates the difference of each timestep with its previous timestep in the latent V space. This term essentially serves as a smoothness constraint penalizing the dissimilarity of neighboring timesteps. The $l_{1,2}$ norm term forces whole column similarity between two columns of V—that is, between neighboring timesteps in V as opposed to just element-wise similarity in the case of a simpler l_1 norm on VR. The solution to Equation (1) can be obtained by applying the alternating direction method of multipliers (ADMM) [15].

Table 1. Definitions

$X \in \mathbb{R}^{n \times m}$	The data matrix consisting of n time series each with m timesteps.
$D \in \mathbb{R}^{n \times n}$	Depicts a degree matrix.
$A \in \mathbb{R}^{n \times n}$	Depicts an adjacency matrix.
$L = D - A$	Represents the Laplacian matrix of A.
$U \in \mathbb{R}^{n \times l}$	Spatial feature matrix with l latent features.
$V \in \mathbb{R}^{l \times m}$	Temporal feature matrix with l latent features. In Equation (1) (i.e., in CnR-V), $l = m$; otherwise (i.e., in CnR-UV), $l << m$ (Equation (5)).
$R \in \mathbb{R}^{m \times m-1}$	A lower triangular matrix with –1's on the primary diagonal and 1's on the second diagonal.
$E \in \mathbb{R}^{n \times k}$	Represents the explanation matrix to quantify importance of each time series in explaining each cut-point.
$\mathbf{1} \in \mathbb{R}^{n \times 1}$	Denotes a vector of 1's.
$\lambda, \alpha, \lambda_i, \gamma_i$	Scalar hyper-parameters used in the segmentation and explanation formulations.

Solving Equation (1) yields a temporal weight matrix $V \in R^{m \times m}$ from which we derive an affinity matrix $W = VV^T$. The affinity matrix is then segmented using the normalized cuts procedure to obtain the set of cut-points S.

3.2 CnR-V Explanation

Recently, there has been a push toward making complex machine learning model outputs quantifiable, explainable, and simple [45]. Despite the sparsity of our segmentation procedure, the output is complex and it is often not possible to identify the cause for each segment due to many simultaneously changing time series. A domain expert may want to know simply which time series are changing and which are behaving anomalously at the sudden outage changes (at each segment). This can help them make decisions about which counties they can use for retrospective analysis by localizing points of failure. Finding out these "culprit" time series using just the temporal and spatial segmentation from V and U matrices seems difficult. Existing time series segmentation algorithms do not provide any explanation of the result in an automatic principled way. Hence, to design good explanations specifically for hurricane outage data, we consider the characteristics of the data and the requirements from the domain experts to propose an optimization problem CnR-V as follows.

PROBLEM 2. *Given a set of time series X, the Laplacian matrix L of the underlying network, a number k, and the k-segmentation of S, find the associated explanations E that capture the main pattern changes in X.*

3.2.1 Overview of Our Approach. We formulate an optimization problem that automatically learns explanations considering the underlying geographical relation between counties, revealing to domain experts a small number of truly important "culprit" counties per cut-point.

3.2.2 Formulation. We aim to design an optimization problem that automatically finds a good set of explanation vectors $\{e_i\}$. Assume that we have a function $d(S, i)$, which takes a segmentation S and a cut-point index i as inputs, and returns an n by 1 vector that captures the difference of each time series before and after the ith cut-point c_i in S. We want e_i to assign higher weights to time series with higher $d(S, i)_j$ values (therefore higher difference across cut-point c_i), where $d(S, i)_j$ represents the importance of county j at cut-point i and is defined in Equation (3). The formulation

also needs to capture the effects of spatial proximity of counties—that is, adjacent counties should have similar importance, due to the continuous trajectory of a hurricane affecting neighboring counties at the same time. The explanation needs to be "simple" in the sense of highlighting only a few culprit counties. With these considerations in mind, the optimization problem we solve to obtain simple explanations considering the county geography is shown next.

Given: A set of time series X, L, a segmentation S, α, λ.
Find: $E = \{e_i\}$ such that

$$\arg\max_E \sum_{i=1}^{k} \left[e_i^T d(S, i) - \alpha e_i^T L e_i \right] - \lambda \sum_{i=1}^{k} ||e_i||_1 \tag{2}$$
$$\text{subject to} \quad 0 \leq e_{ij} \leq 1, ||e_i||_1 = 1$$

The geographical smoothness is introduced in the second term using the Laplacian matrix L (obtained from the underlying county-county network). This term minimizes the difference of e_i for adjacent counties. The third term is an l_1 norm regularization on e_i, which introduces sparsity in e_i leading to simpler explanations due to only a few important counties having non-zero values in e_i to explain cut c_i.

The distance function $d(S, i)$ captures the difference across a cut-point c_i by considering a time window before the cut-point c_i and a time window after c_i. The difference of these two time windows is calculated as the difference of the time series across c_i. Let w_{ij}^- represent the sub-sequence of x_j in the time window before c_i, and let w_{ij}^+ represent the sub-sequence in the time window after c_i. The distance function then calculates the difference of w_{ij}^- and w_{ij}^+ using simple, standard time series features: the mean value (f_1), the standard deviation (f_2), the maximum value (f_3), and the minimum value (f_4).

$$d(S, i)_j = \frac{1}{4} \sum_{z=1}^{4} |f_z(w_{ij}^-) - f_z(w_{ij}^+)| \tag{3}$$

As a preprocessing step that we do not elaborate on in the equation, we perform a min-max normalization of $|f_z(w_{ij}^-) - f_z(w_{ij}^+)|$ across all time series to make the scales uniform. As both w_{ij}^- and w_{ij}^+ are of a short length (a deliberate setting since the pattern changes that justify the choice of a particular cut-point usually lie in the local area), these simple features are enough to capture the main pattern difference.

Finally, to solve Equation (2), we optimize each e_i separately. For each e_i, the optimization can be rewritten as a quadratic programming (QP) problem in the following way.

$$\arg\min_{e_i} \quad \alpha e_i^T L e_i - [d(S, i)^T - \lambda \mathbf{1}^T] e_i \tag{4}$$
$$\text{subject to} \quad 0 \leq e_{ij} \leq 1, ||e_i||_1 = 1$$

The QP problem is well studied in the literature, and it is NP-hard in its general form. In our case, where the QP is convex in e_i, it can be solved in polynomial time using an interior point method [57], and we use the existing Matlab function (quadprog) to solve the problem.

4 SPATIO-TEMPORAL CUT-N-REVEAL

We now augment our CnR methodology to incorporate spatial relationships into the temporal segmentation and explanation phases and propose our novel CnR-UV model.

4.1 CnR-UV Segmentation

Modeling the power outage failure process using CnR-V presents a few drawbacks. First, the segmentation process in Equation (1) does not account for or attempt to model spatial relationships

between entities (counties in our case) over which the failure process (power outage) occurs. However, phenomena like cascading failures indicate the existence of strong spatial interactions between components in the power grid, and incorporating spatial relationships can aid in more effective modeling of the power outage process. We update Problem 1 stated in Section 3.1 as follows.

PROBLEM 3. *Given a set of time series X, the Laplacian matrix L of the underlying spatial network, and a number k, find a spatial weight matrix U, a temporal weight matrix V, and the k-segmentation of S derived from V that captures the main temporal pattern changes in X.*

4.1.1 Overview of Our Approach. For effective spatio-temporal modeling, we allow temporal latent matrix V to consider the underlying spatial relationships between counties. To this end, we introduce a spatial weight matrix U, jointly learned with V. U, V are latent weight matrices, and the latent factor modeling approach is used for our segmentation model because of its success in similar sparse settings like recommendation systems [30, 38].

4.1.2 Formulation. We develop a temporal segmentation formulation influenced by spatial constraints, where the failure process at each timestep is represented in a rich low-dimensional latent space l such that $V \in \mathbb{R}^{l \times m}$, $U \in \mathbb{R}^{n \times l}$, and $l << m, l << n$. Let $v_i \in \mathbb{R}^{l \times 1}$ and $v_j \in \mathbb{R}^{l \times 1}$ represent the ith and j^{th} column vectors of V, respectively, where $i, j \in \{1, \ldots, m\}$ and $i \neq j$. We can also consider v_i and v_j to be the latent representation for the ith and j^{th} timesteps, respectively. The goal of this formulation is that the similarity of v_i, v_j is not solely influenced by the temporal proximity of v_i to v_j (a constraint strongly enforced by the $||VR||_{1,2}$ term in Equation (1)) but also by the underlying spatial behavior of the counties at timesteps i and j. To achieve this goal, we formulate a novel temporal segmentation model in Equation (5) to jointly model spatial and temporal characteristics of power outage during natural disasters.

$$\min_{U,V} \frac{1}{2}||X - UV||_F^2 + \lambda_1||U||_1 + \frac{\beta_1}{2}Tr(U^T L U)$$
$$+ \lambda_2||V||_1 + \lambda_3||VR||_{1,2} \tag{5}$$
$$\text{subject to} \quad U \geq 0, V \geq 0$$

In Equation (5), the matrix U learns the latent representation for each of the n counties. The first term calculates the reconstruction error wherein the original failure behavior observed in X is recreated as a combination of U (latent county outage characteristics) and V (latent temporal outage characteristics). The l_1 norm terms on U and V ensure sparsity, in line with our goal of designing simple interpretable explanations of our segmentation. The $||VR||_{1,2}$ term has the same effect as described in Section 3.1. The term $Tr(U^T L U)$ represents the Laplacian regularization constraining the matrix U to be influenced by the underlying geographical layout of the counties in X. Here, the matrix L represents the Laplacian of the county-county adjacency matrix A.

We once again employ the ADMM method to solve Equation (5) using the Lagrangian formulation as represented in Equation (6). To separate each term in Equation (5), we assign $J = U, K = V$, $P = KR$.

$$\mathcal{L}(U, V, J, K, P) = \frac{1}{2}||X - JK||_F^2 + \lambda_1||U||_1 + \frac{\beta_1}{2}\mathbf{Tr}(J^T L J)$$
$$+ \lambda_2||V||_1 + \lambda_3||P||_{1,2} + \langle G, V - K \rangle + \frac{\gamma_1}{2}||V - K||_F^2$$
$$+ \langle H, U - J \rangle + \frac{\gamma_2}{2}||U - J||_F^2 + \langle F, P - KR \rangle \tag{6}$$
$$+ \frac{\gamma_3}{2}||P - KR||_F^2$$

We solve for U, V, J, K, P in an alternating manner. The update steps for each term in Equation (6) are discussed next:

(1) *Update V:*

(a) Fixing U, J, K, P, we solve for V.

$$\min_V \quad \lambda_2||V||_1 + \langle G, V - K \rangle + \frac{\gamma_1}{2}||V - K||_F^2$$

This can be restated as follows.

$$\min_V \quad \lambda_2||V||_1 + \frac{\gamma_1}{2}||V - \left(K - \frac{G}{\gamma_1}\right)||_F^2 \tag{7}$$

Equation (7) has element-level closed-form solutions that can be obtained using the soft thresholding operator [10, 34, 52]. The element-level closed-form solution is as defined in Equation (8).

$$V = sign\left(K - \frac{G}{\gamma_1}\right) \ max\left(\left|K - \frac{G}{\gamma_1}\right| - \frac{\lambda_2}{\gamma_1}\right) \tag{8}$$

(b) Fixing U, V, J, P, we solve for K.

$$\min_K \frac{1}{2}||X - JK||_F^2 + \langle G, V - K \rangle + \frac{\gamma_1}{2}||V - K||_F^2$$
$$+ \langle F, P - KR \rangle + \frac{\gamma_3}{2}||P - KR||_F^2 \tag{9}$$

Differentiating Equation (9) w.r.t. K and setting the derivative to zero yields the following.

$$(X^T J^T JX + \gamma_1 I)K + \gamma_3 KRR^T$$
$$= X^T JX + G + \gamma_1 V + FR^T + \gamma_3 PR^T \tag{10}$$

If we set

(i) $A = (X^T J^T JX + \gamma_1 I)$
(ii) $B = \gamma_3 RR^T$
(iii) $C = X^T JX + G + \gamma_1 V + FR^T + \gamma_3 PR^T$,

then Equation (10) takes the form of a Sylvester equation.

$$AK + KB = C \tag{11}$$

The solution to Equation (11) is a well-studied problem. [13, 24].

(c) Fixing U, V, K, J, we solve for P.

$$\min_P \lambda_3||P||_{1,2} + \langle F, P - KR \rangle + \frac{\gamma_3}{2}||P - KR||_F^2 \tag{12}$$

This is equivalent to the following.

$$\min_P \lambda_3||P||_{1,2} + \frac{\gamma_3}{2}\left\|P - \left(KR - \frac{F}{\gamma_3}\right)\right\|_F^2 \tag{13}$$

Let $M = KR - \frac{F}{\gamma_3}$, then Equation (13) has the following closed form solution [52].

$$P(:, i) = \begin{cases} \frac{||M(:,i)|| - \frac{\lambda_3}{\gamma_3}}{||M(:,i)||} M(:, i) & if \ ||M(:, i)|| > \frac{\lambda_3}{\gamma_3} \\ 0 & otherwise \end{cases} \tag{14}$$

(2) *Update U*:
   (a) Fixing V, J, K, P, we solve for U. We can follow a similar procedure to the preceding V update step and obtain the following element-wise closed-form solution for U.

$$U = sign\left(J - \frac{H}{\gamma_2}\right) \ max\left(\left|J - \frac{H}{\gamma_2}\right| - \frac{\lambda_1}{\gamma_2}\right) \tag{15}$$

   (b) Fixing U, V, K, P, we solve for J.

$$\min_J \frac{1}{2}||X - JK||_F^2 + \frac{\beta_1}{2}Tr(J^T LJ) + \langle H, U - J\rangle$$
$$+ \frac{\gamma_2}{2}||U - J||_F^2 \tag{16}$$

Differentiating Equation (16) w.r.t. J and setting the derivative to 0 similar to the K update procedure, the expression in Equation (17) is obtained.

$$\beta_1 LJ + J(XKK^T X + \gamma_2 I) = XKX^T + H + \gamma_2 U \tag{17}$$

We once again solve Equation (17) by reduction to a Sylvester equation:
   (i) $A = \beta_1 L$
   (ii) $B = XKK^T X + \gamma_2 I$
   (iii) $C = XKX^T + H + \gamma_2 U$
(3) *Update G*:

$$G = G^{old} + \gamma_1(V - K)$$

(4) *Update H*:

$$H = H^{old} + \gamma_2(U - J)$$

(5) *Update F*:

$$F = F^{old} + \gamma_3(P - KR)$$

(6) *Update $\gamma_1, \gamma_2, \gamma_3$*:

$$\gamma_1 = \rho\gamma_1^{old}; \gamma_2 = \rho\gamma_2^{old}; \gamma_3 = \rho\gamma_3^{old}$$

Solving Equation (6) yields an $l \times m$ temporal weight matrix V and an $n \times l$ spatial weight matrix U. We construct an affinity matrix $W = V^T V$ that is passed to the normalized cuts algorithm to obtain the temporal segmentation S from V. As an additional step, we also construct a separate spatial affinity matrix $W_U = UU^T$ that represents county similarity and obtain a spatial clustering of W_U using the normalized cuts procedure. In addition to the temporal segmentation and the explanation of each temporal segment, we believe that the spatial clustering of counties provides an additional level of insight about aggregate county behavior during natural disasters in a given region.

4.2 CnR-UV Explanation

The explanation procedure for model CnR-V proposed in Section 3.2 incorporates spatial constraints through the Laplacian of the county adjacency matrix. In our experience, this approach overly emphasizes spatial locality as a factor for learning the explanation vector e_i for a particular cut-point c_i. It need not always be the case that the effects of a power outage in a particular county are felt only in the neighboring counties or that only counties directly affected by a hurricane experience outages. As outlined in the work of Hines et al. [27], the influence graph for a county power outage need not necessarily be exactly similar to the grid topology or geographical county

layout. Intuitively, this means that outage in a county in one part of a state can have far-reaching effects leading to outages or in counties located in a different part of the state in an instantaneous or delayed manner. Accommodating for such effects in our explanation methodology requires a smoother, less stringent spatial constraint. This leads to better explanations for domain experts as well.

4.2.1 Overview of Our Approach. In addition to the V matrix, the segmentation formulation of the CnR-UV model also learns a rich latent factor representation of each disaster-affected county U. Due to the richness of the latent factor representation and flexibility of design, the U matrix, in addition to local spatial effects, is also able to capture far-reaching effects of counties on each other. Hence, the affinity matrix UU^T would capture far-reaching county-county similarities extending significantly beyond the immediate neighborhood of a county. We utilize this property and construct $W_U = UU^T$, which can be considered the adjacency matrix of a weighted undirected graph of counties whose degree matrix D is a diagonal matrix where each D_{jj} represents the weight of county j and is calculated as the sum of row j of W_U. Matrix L_U is the Laplacian calculated as $L_U = D - W_U$.

PROBLEM 4. *Given a set of time series X, a number k, the k-segmentations of S, and the Laplacian L_U derived from the spatial latent factor matrix U, find the associated explanations E that capture the main pattern changes in X.*

4.2.2 Formulation. The explanation formulation employed by CnR-UV is defined in Equation (18). It is similar to Equation (2) but for a smoother Laplacian matrix L_U in the regularization term that allows e_i to consider counties in a larger spatial radius as opposed to the explanation step of CnR-V wherein a strict spatial constraint based on the county graph is imposed through the Laplacian matrix L.

$$\arg\max_E \sum_{i=1}^{k} \left[e_i^T d(S, i) + \alpha e_i^T L_U e_i \right] - \lambda \sum_{i=1}^{k} ||e_i||_1 \tag{18}$$
$$\text{subject to} \quad 0 \le e_{ij} \le 1, ||e_i||_1 = 1$$

The function $d(S, i)$ returns an explanation vector $e_i \in \mathbb{R}^{n \times 1}$ and is defined in Equation (3). Equation (18) can be solved by optimizing each e_i as a separate QP problem convex in e_i similar to the explanation formulation for CnR-V in Section 3.2. The complete pseudo-code for CnR-UV is given next (CnR-V is similar, using Equation (1), Equation (4) instead of Equation (6), and Equation (18) respectively).

ALGORITHM 1: CnR-UV Segmentation with Explanation

Input: X: Hurricane Power Outage Data, G: Spatial Graph, l: Num. Latent Features
Result: $S = \{c_1, \ldots, c_k\}$, Temporal Segmentation
$E = \{e_{c_1}, \ldots, e_{c_k}\}$, Temporal Explanation
Init: U = V = 0
while *not converged* **do**
    | Estimate, U, V using Equation (6)
    | Retrieve S using Normalized Cuts
    | Estimate explanation vectors $e_{c_1}, \ldots, e_{c_k}$ using Equation (18)
end

Remark 1. CnR-UV takes worst-case time $O(\#iter l^2 (X + m^2 + n^2)))$ and is quadratic in the number of time steps and time series. In practice, we found QP to be very fast and total time to be sub-quadratic on the dataset size. CnR-V takes worst-case time $\sim O(\#iter(m^{2.3} + n^2))$ (using the best

Table 2. Datasets Used

Dataset	#Time stamps	#Time Series	Ground Truth
Synthetic	1,000	4	✓
NILM	721	17	✓
ChickenDance 1	1,590	4	✓
ChickenDance 2	322	4	✓
WalkJog 1	1,000	2	✓
WalkJog 2	303	2	✓
GrandMal	1,000	2	✓
Harvey	264	250	
Irma	169	271	
Matthew	252	369	

matrix multiplication exponent) and is hence sub-cubic in the number of timesteps and quadratic in the number of time series. The space complexity of CnR-UV is near-linear $O(X + nl + ml)$, and that of CnR-V is $O(X + m^2 + n^2)$.

5   EMPIRICAL STUDY

We implement CnR in Python and Matlab. Our experiments were conducted on a 4 Xeon E7-4850 CPU with 512 GB of 1,066-Mhz main memory.

5.1   Setup

5.1.1   Datasets. We collect datasets from different domains with the ground-truth segmentations to quantitatively evaluate our performance. For efficiency purposes, we perform a standard rolling average as a preprocessing step to all of the data. The final statistics are in Table 2.

ChickenDance. The *ChickenDance* datasets, *ChickenDance1* and *ChickenDance2* [17], are recorded as motion capture sequences of 4-dimensional data points with ground-truth segmentation [35] and is originally from the CMU motion capture database [2]. The ground-truth segmentation is based on different motions in the chicken dance.

WalkJog. We used two variants of the *WalkJog* datasets, *WalkJog1* where we uniformly sampled 1,000 data points from the *WalkJog* dataset used in [23] and *WalkJog2* used in the work of Chen et al. [18]. These datasets adapted from the REALDISP activity recognition dataset [11] have recordings of walking and jogging motions with segments between different motions.

GrandMal Seizures. Gharghabi et al. [23] have 3-minute recordings of neural activity (pre-seizure, seizure, and post-seizure) of a subject, recorded using a scalp electrode.

Synthetic Data. We also generated synthetic data consisting of four time series sampled from normal distributions with different means and standard deviations. Time series were perturbed at different times to cause segments, and the goal is to identify these segments.

NILM. The non-intrusive load monitoring dataset (NILM) consists of real power measurements for various household appliances like lamps, laptops, and refrigerators, recorded through the use of measurement and actuation units (MAUs) connected between the device and the wall socket (more details are found in the work of Reinardt et al. [44]). We use a 24-hour hour snapshot of the

NILM data from 2012-01-17 00:00:00 to 2012-01-17 23:59:59 sampled at 2-minute intervals and use the time when a device switches states as the ground-truth cut-points.

Hurricane Outage data. ORNL has developed several grid situational awareness products over the past decade such as VERDE, EARSS, and EAGLE-I [19] for different stakeholders like DOE and FEMA, primarily for emergency management. For example, the National Outage Map within EAGLE-I collects distribution outage data of all customers from utility websites every 15 minutes. Due to the recent coverage expansion (with more utilities exposing data from their Outage Management Systems), in this work we consider the more recent hurricane outage data namely for Matthew, Harvey, and Irma since it covers nearly 90% of the population in the hurricane-affected areas.

5.1.2   Baselines. We wish to evaluate the *segmentation* and *explanation* parts of our CnR-UV algorithm. We first start with evaluating the performance of the CnR-UV segmentation procedure and later detail the CnR-UV explanation evaluation.

5.1.3   Segmentation Baselines. First, we compare the segmentation of CnR-UV with several state-of-the-art multivariate time series segmentation algorithms.

AutoPlait [35] is a hidden Markov model (HMM)-based algorithm that discovers different regimes in co-evolving time series. Each regime can be thought of as the segments for our problem.

TICC [25] is a recent algorithm for multivariate time series to discover repeated patterns. It clusters timestamps into segments using their model.

DynaMMo [32] learns a dynamical system (Kalman filter) and segments the time series wherever the reconstruction error becomes high.

Floss [23] is an unsupervised semantic segmentation algorithm that learns the segmentation from the local minimas obtained in the matrix profile.

5.1.4   Explanation Baselines. To the best of our knowledge, there is no method that retrieves explanations for each segment the way CnR-UV does. Hence, we are unable to compare CnR-UV explanations with those of other state-of-the-art algorithms. We do, however, evaluate explanation performance for the aforementioned datasets with ground-truth segments. The evaluation procedures for segmentation and explanation are detailed in Section 5.2.

5.2   Quantitative Evaluation

5.2.1   Segmentation. We compare CnR-UV performance with several segmentation baselines on datasets with ground-truth segmentations: *NILM*,*ChickenDance*,*Synthetic*,*GrandMal*, and *WalkJog*. We evaluate the detected cut-points by calculating the F1 score based on the ground-truth cut-points (as in the work of Matsubara et al. [35]). Higher F1 scores indicate better segmentation. For all of our experiments with CnR-UV, we set $l = 2$ (our algorithm was robust to varying latent factor dimensions) and chose the hyper-parameters using *gridsearch*. We show the results in Table 3, where we observe that CnR-UV outperforms all methods on most datasets except *GrandMal* and *WalkJog1*. The F1 score corresponding to the best segmentation model per dataset is highlighted in bold. To visually inspect the CnR-UV segmentation, we depict segmentation results in Figure 2 for *ChickenDance1*, *WalkJog2*, and *Synthetic* datasets where CnR-UV performs the best. For *ChickenDance1* in Figure 2(b), CnR-UV is able to isolate all of the different data trends successfully. It correctly identifies all of the seven ground-truth cut-points, and the remaining cut-point at timestep 13 (red dashed line) is a false positive. In Figure 2(a), for *WalkJog2*, we see that CnR-UV correctly separates the sequences of data generated due to walking from those due to jogging. Time series segmentation models are less affected by the number of time series in the model and more by the degree and frequency of perturbation of the time series. We can see in Table 3

Table 3. Evaluation of Segmentation (Seg) and Explanation (Exp)
on Ground-Truth Datasets Based on the F1 Score

Method Dataset	CnR-UV seg	CnR-UV exp	CnR-V	Auto Plait	TICC	Dyn.	Floss
Synthetic	**1.0**	1.0	0.58	0.5	**1.0**	0.52	0.85
NILM	**0.83**	1.0	0.56	0.4	0.82	0.71	0.73
Chicken1	**0.93**	1.0	0.63	0.85	0.92	0.54	0.53
Chicken2	**0.85**	1.0	0.73	0.73	0.5	0.75	0.71
WalkJog1	0.22	1.0	0.57	0	0.86	0.54	**1.0**
WalkJog2	0.75	1.0	**1.0**	0	0.33	0	0
GrandMal	0.86	1.0	0.58	0.5	**1.0**	0.36	0.5

(a) *WalkJog.*   (b) *ChickenDance.*   (c) *Synthetic.*
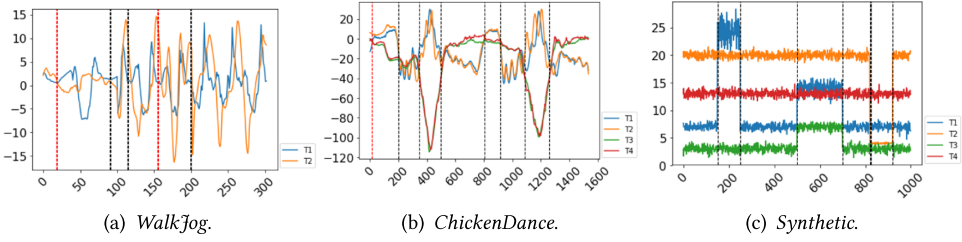
Fig. 2. CnR-UV segmentation results (vertical dashed lines) for the *Walkjog2*, *ChickenDance1*, and *Synthetic* datasets. True positive segments are colored black, and false positives are colored red. We consider all segments within the tolerance window (5% of total timesteps) of the ground-truth segments as true positive.

that CnR-UV performs well in cases where the number of time series is high (e.g., NILM). Each cut-point discovered by our method lies in a 5% cut-point location tolerance window with respect to the ground-truth cut-point, and we adopt this practice from previous literature [17, 35].

5.2.2 Explanation. CnR-UV is also able to retrieve reasonable explanations for proposed segmentations in each case. Since there is no existing literature performing explanation in an automatic and principled way, we were unable to compare our explanation algorithm with other baselines. In addition, since we did not have any ground truth for explanations, we created a ground-truth dataset by manually generating explanations for each cut-point. We did this by identifying a subset k_i of the n time series in a dataset that experienced perturbation across a cut-point c_i. This subset k_i of time series can be considered the ground-truth explanation for cut-point c_i. We then compare the top $|k_i|$ (cardinality of set k_i) values in the explanation vector e_i against the ground-truth explanations using the F1 score. This is repeated for all cut-points, and an average F1 score is calculated for explanations on the dataset. Results of this procedure are outlined for each dataset in Table 3 (CnR-UV exp). Explanations were evaluated on *ChickenDance*, *WalkJog*, *NILM*, *Synthetic*, and *GrandMal* datasets. We only consider true-positive segments identified by CnR-UV while calculating explanation F1 scores. For the *WalkJog1* dataset, even though CnR-UV segmentation is low (F1 score = 0.22), our explanation performs well (F1 score = 1.0). This is because we only use the true-positive segments and calculate explanations for those segments because of the availability of ground-truth explanation data only for true-positive segments.

5.2.3 Discussion of CnR-UV Compared to Other Baselines. For the best performance, CnR-UV models should be provided with the spatial graph relating the time series being modeled.

CnR-UV was so designed, bearing in mind the goal of modeling power system failure processes during hurricanes using real-world data. However, to holistically evaluate temporal segmentation performance, we compared CnR-UV to many state-of-the-art baselines on several datasets. In this context, all time series were considered spatially independent (as we did not have prior knowledge of spatial inter-dependencies). Due to this lack of spatial information, CnR-UV underperformed as the U matrix was unable to learn the best possible representation. Despite this, our model matches or outperforms strong baselines like *TICC*, *DynaMMo*, *AutoPlait*, and *Floss* in five out of seven datasets. It must be noted that despite the lack of spatial information, CnR-UV also outperforms the CnR-V model on five out of seven datasets (Table 3), indicating that the low-dimensional latent factor U and V matrices in CnR-UV are indeed able to learn rich representations of the failure process compared to the large sparse square V matrix as in the case of CnR-V. In the datasets where spatial information is missing, we treat all time series as independent. The reason for the under-performance of CnR-UV in *Walkjog* and *GrandMal* datasets w.r.t. *TICC* may have to do with this time series independence assumption being sub-optimal.

DynaMMo performs segmentation based on reconstruction error w.r.t. a tolerance threshold specified by the user. We found that the segmentation was sensitive to this tolerance threshold parameter, which directly governs the number of segments allowed. In most cases, *DynaMMo* was found to over-segment or under-segment depending on the error tolerance.

In the case of the *AutoPlait* model, it is found to perform better on datasets with less spiky (sudden) changes in time series. For example, if we observe Figure 2, the *WalkJog* and *Synthetic* dataset time series have a much more spiky and sudden changing behavior than the *Chicken-Dance* dataset. However, in the case of the *ChickenDance* dataset, although Figure 2(b) shows spikes around timesteps 400 and 1,200, the rest of the patterns are either increasing or decreasing trends that are relatively non-spiky in nature.

Floss performs segmentation in multivariate time series by finding local minima on the average CAC curve [23]. Thus, for *GrandMal* and *ChickenDance1* data where multiple groups of time series exhibit large and sometimes spiky changes at different timesteps, the CAC curve of all time series do not exhibit local minima at the same or close timesteps. This results in the average CAC curve not yielding local minima at all of the ground-truth cut-points, which causes the low F1 scores for *Floss* in Table 3. In addition, we must note that the *ChickenDance2* dataset is smoother than *ChickenDance1* (i.e., changes are smaller/more gradual than *ChickenDance1*), and we immediately see a significant performance improvement in this scenario in the F1 score of *Floss*.

We will now present real-world applications of CnR-UV on several hurricane power outage datasets as case studies. We characterize both CnR-UV segmentation and explanation procedures on all hurricane datasets.

5.3 Case Studies: Hurricanes

In Section 2, we set out to design a model to address the following goals:

(1) Identify phases of a hurricane as a function of severity of damage to critical infrastructure like the power grid.
(2) Identify the most important counties that characterize each phase (i.e., "explain" each phase).
(3) Group counties together based on their overall failure dynamics through the hurricane, to allow for overall assessment of the spatial span of the damage.

With the aforementioned goals in mind, we ran CnR-UV for power outage failure data from three recent hurricanes. We show that CnR-UV can find meaningful pattern changes and insightful associated explanations. Specifically, the current culprit definition can be used to distinguish between

(a) Irma CnR-UV segmentation

(b) Spatial cluster

(c) Important
time series for c_1

(d) Important
time series for c_2

(e) Important
time series for c_3

(f) Important
time series for c_4

(g) Important
time series for c_5

(h) Explanation e_1

(i) Explanation e_2

(j) Explanation e_3

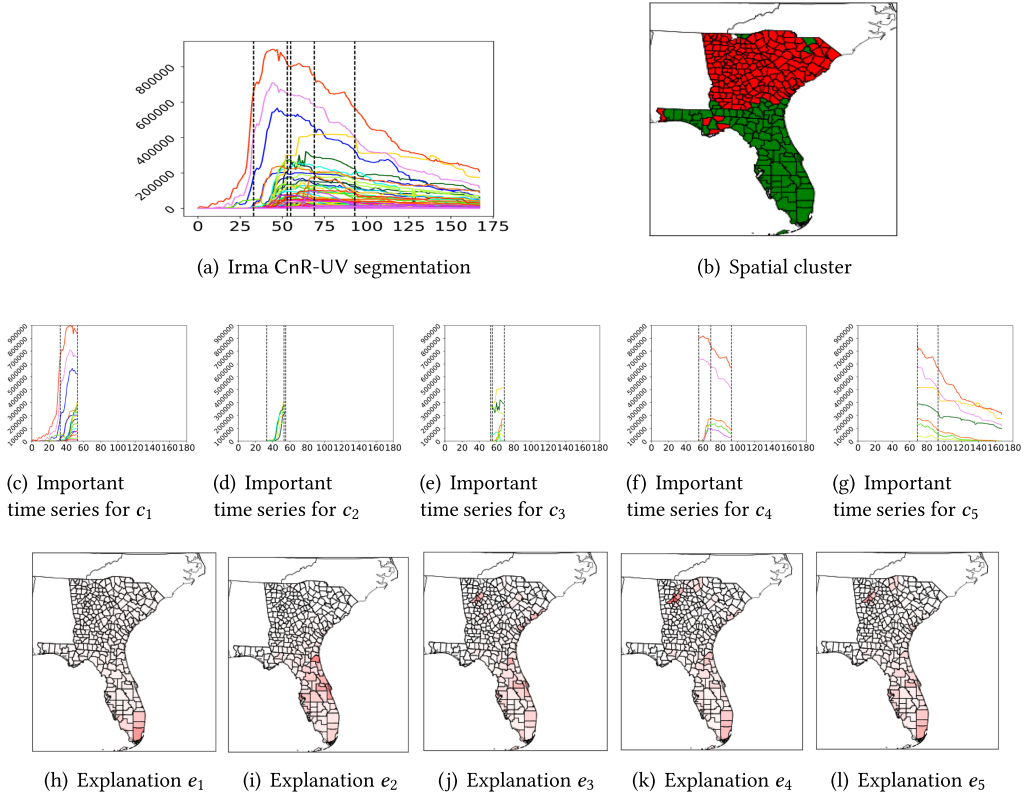(k) Explanation e_4

(l) Explanation e_5

Fig. 3. Segmentation and the corresponding explanations for Irma. (a) All counties with grid failures during Hurricane Irma are shown. Each county is represented by a time series with an individual color in a solid line. The vertical dashed lines are the cut-points obtained by CnR-UV. (b) The spatial clustering result shows the spatial span of grid failure, based on spatial proximity of counties and similarity in failure patterns of their time series. (c–g) The most important time series for each cut-point in the segmentation obtained from e_i whose explanation weight is >0.1. (h–l) e_i visualizations in geographical space for each cut-point. Counties with higher e_i values (higher values represented by darker red) are more important for the cut-point and are marked with a color closer to red.

regimes while also being applicable to the hurricane failure setting where the failure process of each county follows a typical increasing, peak, decreasing trend pattern. This is because multivariate hurricane failure time series are highly complex. Although the failure pattern (increasing failure rate, peak, decreasing failure rate) is consistent across counties, the time of failure and rate of failure differ widely across counties requiring a formulation as defined by us in Equation (5) to capture the complexities (and local changes around cut-points) of this spatio-temporal multivariate failure process. The effectiveness of our model in capturing complex patterns in multiple hurricanes will be demonstrated in the following section. For the segmentation model, we set the number of latent dimensions (*l*) to 5, and for each cut-point, we consider counties with explanation weight > 0.1 as important.

5.3.1 Hurricane Irma. We show the results in Figure 3. Figure 3(a) represents the overall segmentation that CnR-UV yields for Hurricane Irma, whereas Figure 3(c) through (g) show the explanations yielded by CnR-UV across each cut-point in the segmentation. All explanation figures (except those for the first and last cut-point) consist of three cut-points—that is, the cut-point being

explained, along with the previous and the next cut-point. Each explanation figure is accompanied with a spatial visualization of the important counties highlighted by the explanation of the cut-point. Figure 3(h) through (l) are spatial depictions of the explanations in Figure 3(c) through (g), respectively. Finally, Figure 3(b) represents clustering results of the spatial matrix U. All of the following hurricane result visualizations are organized in the same manner.

The first cut-point (showcased in Figure 3(c)) at timestep 35 (around September 10) shows hurricane landfall when the outages of a few counties seem to rise sharply. Indeed, Figure 3(h) shows these counties at the southern tip of Florida indicating the location of landfall of Hurricane Irma. The second and the third cut-points in Figure 3(a) might seem redundant owing to their close proximity. However, the second cut-point (showcased in Figure 3(d)) is capturing a small rising trend of county power outages for the counties highlighted in Figure 3(i). However, the third cut-point captures fluctuations and plateaus in a different set of counties. The fourth cut-point c_4 (and the corresponding explanation e_4) (Figure 3(f) and (k)) is interesting: first, it captures a short rising outage trend (of smaller magnitude) at Dekalb, Fulton, and Gwinnett counties in the Northwest. One report [3] suggest that this is due to a separate tropical storm. At the same time, it also captures the start of the decrease in outages at Miami and Broward counties, both of which rise at the beginning in the first cut-point. Thus, CnR-UV can correctly capture the power restoration period of these counties (Miami and Broward) automatically. The last cut-point c_5 (and corresponding explanation e_5) at timestep 93 (around September 12) captures the date when Hurricane Irma was downgraded to a category 2 storm and the outages of the counties started to decrease. Note that these cut-points and explanations are non-trivial, and are successfully modeled since CnR-UV is able to capture the diverse trends in power outages of different magnitudes including in faraway counties that do not follow the hurricane trajectory. As mentioned in Section 1, retrospective analysis of hurricanes through CnR-UV helps capture failure and restorative phases (e.g., Miami and Broward counties) through *segmentation*, which can help experts understand grid resilience and restoration patterns. At the same time, CnR-UV *explanations* in addition to pin-pointing hurricane-affected regions that incurred major power outages can also uncover subtle trends in regions where consequential events occur, such as the tropical storm at Dekalb, Fulton, and Gwinnett that was caught by CnR-UV explanations. Such insights can alert grid maintainers about the potential for such situations in the future.

Spatial clusters. Figure 3(b) shows the spatial clustering of all counties affected by Hurricane Irma (i.e., the clustering based on W_U, where $W_U = UU^T$ is the spatial affinity matrix as explained in Section 4.2.1). It turns out that the green cluster contains counties most affected by power outages, whereas the red cluster shows the counties whose power outages were comparatively lower. This extent of the green cluster (toward the western/northwestern part) is challenging to estimate by hand or through physical surveys but has been uncovered by CnR-UV solely based on time series dynamics and spatial constraints. This ultimately can aid disaster management experts and power companies to plan recovery for future hurricanes [16, 39].

5.3.2 *Hurricane Harvey.* The CnR-UV results for Hurricane Harvey are depicted in Figure 4. The spatial depiction of explanations in Figure 4(g) through (j) broadly trace the trajectory of the hurricane along the eastern coast of Texas, with a few additional non-coastal counties also being highlighted as important in the northern and northwestern parts of Texas.

In Figure 4(a), the first and the second cut-point might seem redundant owing to their close proximity, and their both capturing increasing outage trends. However, upon closer investigation, we find that the first cut-point is detected when there is a sharp spike in El Paso and Howard counties at the very beginning of the hurricane. As no other counties have begun to experience outages

(a) Harvey CnR-UV segmentation

(b) Spatial cluster

(c) Important time series for c_1

(d) Important time series for c_2

(e) Important time series for c_3

(f) Important time series for c_4

(g) Explanation e_1

(h) Explanation e_2

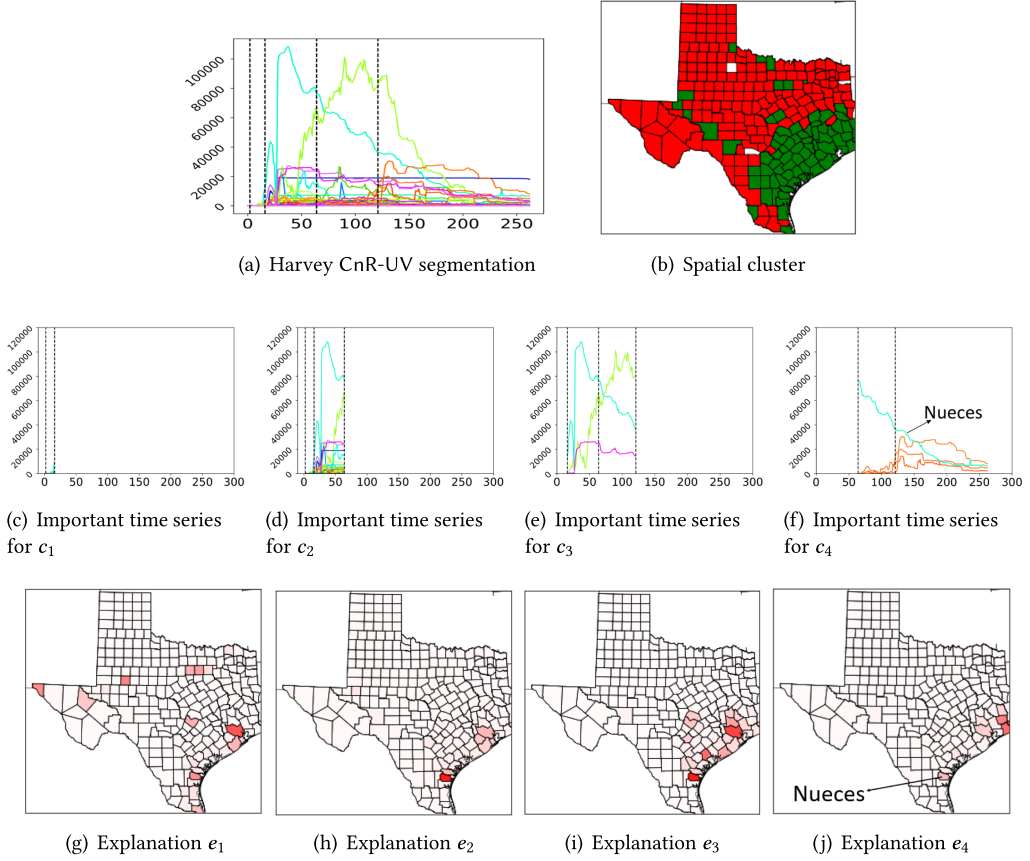(i) Explanation e_3

(j) Explanation e_4

Fig. 4. Segmentation and the corresponding explanations and spatial clustering for Hurricane Harvey obtained by CnR-UV analogous to Figure 3. See detailed discussions in Section 5.3.2.

at this point, even the relatively low absolute values of power outages (around 1,600 homes) are captured by our segmentation model, leading to the first cut-point.

The spatial explanation Figure 4(g) depicts as important a few disconnected counties in the northern and northwestern part of Texas, which might seem counter-intuitive at first. However, reports [1, 4] suggest that these counties were hit by floods as a result of Hurricane Harvey causing major damage.

Similarly, the explanation of the second cut-point (Figure 4(d)) highlights the spike in outages at Nueces and Aransas (around 100,000 homes) but also captures Fort Bend, Brazoria, and Harris (Figure 4(h) groups three counties highlighted in the northern part of the east coast of Texas) as important. Although their outages are low (around 2, 000) compared to Nueces, they have a very sharp peak at this cut-point. One report [5] states that the sudden rise of this peak is due to an EF1-level tornado on August 26, which caused major damage at Fort Bend and also potentially affecting the surrounding counties.

The explanation for the third cut-point (Figure 4(e)) captures two different patterns: the high outage spike of Harris County (green line) and the declining trend at Victoria and Nueces counties. Finally, for the last cut-point (Figure 4(f)), although the outages in many counties are decreasing, our algorithm correctly highlights a sudden rise of outages in Orange, Jefferson, and Hardin

(a) Matthew CnR-UV segmentation

(b) Spatial cluster

(c) Important time series for c_1

(d) Important time series for c_2

(e) Important time series for c_3

(f) Important time series for c_4

(g) Explanation e_1

(h) Explanation e_2

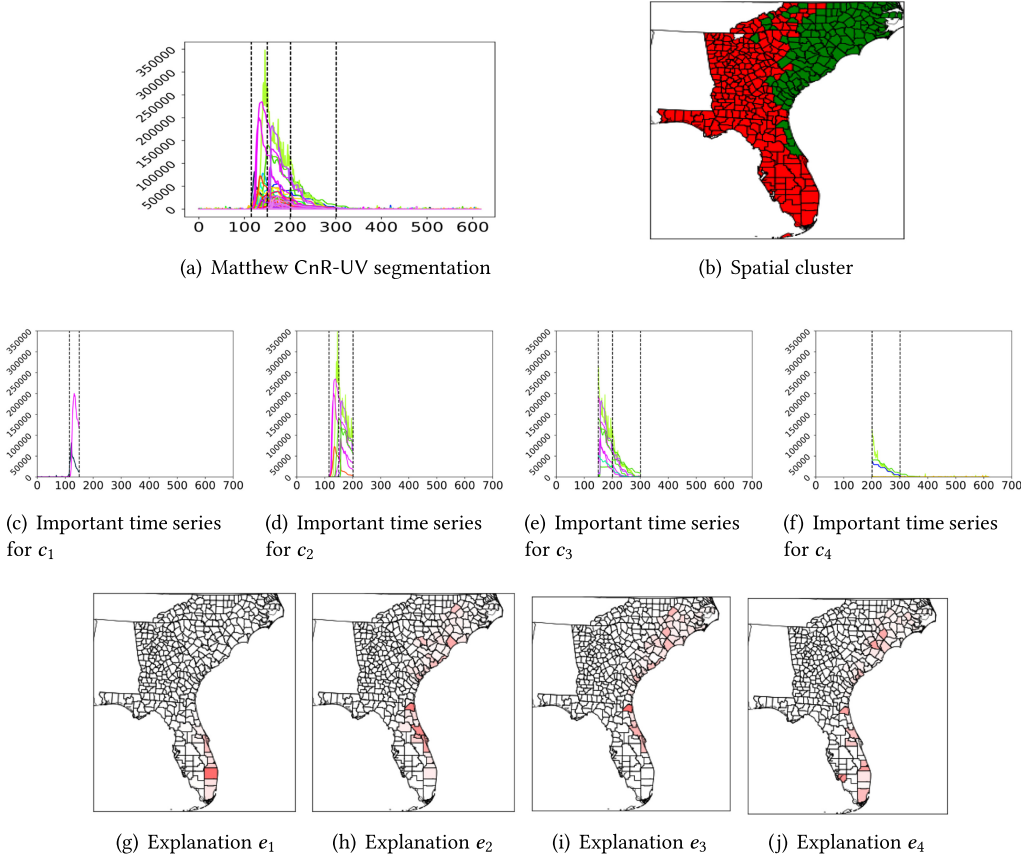(i) Explanation e_3

(j) Explanation e_4

Fig. 5. Segmentations and the corresponding explanations and spatial cluster results for Hurricane Matthew obtained by CnR-UV analogous to Figure 3.

counties. The main reason for this increase is due to the rising water of the Neches River, which causes the city to lose service from its major pump stations. As in the case of Irma, spatial clustering results for Hurricane Harvey (Figure 4(b)) also help us glean the overall picture of the spread of damage due to the hurricane. This explanation is beneficial for doing an inter-dependency study. Note that CnR-UV captures long-range county dependencies even if the counties are not geographically close to each other; such information of subtle county relationships is often buried deep in the original set of hundreds of time series and cannot be uncovered through simple models or through rudimentary visual or statistical analysis of the original data.

5.3.3 Hurricane Matthew.
Similar to previous results, CnR-UV is able to extract insightful cut-points and explanations of all of the major regimes of Hurricane Matthew.

Cut-point 1 (Figure 5(c)) captures the phase of hurricane landfall (October 2). However, CnR-V does not capture the bottom-most southern county depicted in Figure 5(g), whereas CnR-UV successfully captures this, thereby yielding a more holistic explanation of the cut-point.

Cut-point 2 (Figure 5(d)) is detected because of the high rise of peak outages in Chatham (October 4). The spatial representation of the explanation in Figure 5(h) highlights counties along the trajectory of the hurricane.

(a) Harvey CnR-V segmentation

(b) Important timeseries for c_1

(c) Important timeseries for c_2

(d) Important timeseries for c_3

(e) Explanation e_1

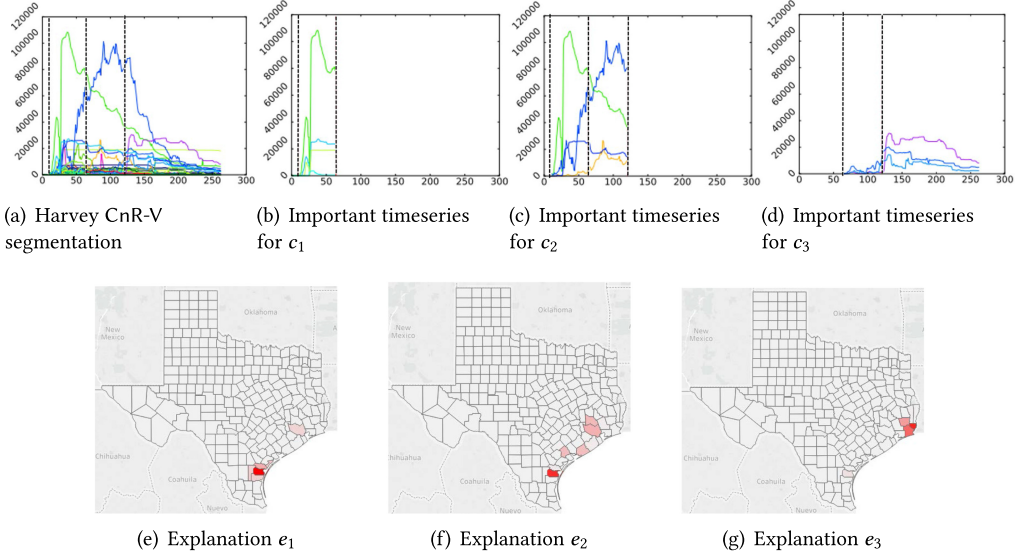(f) Explanation e_2

(g) Explanation e_3

Fig. 6. Segmentations and explanations results of CnR-V for Hurricane Harvey analogous to Figure 3.

Cut-point 3 (Figure 5(e)) captures the high decrease of outages, which captures the restoration of Chatham, Duval, and so forth. At the same time, this cut-point is capturing a sudden rise of outages of Horry County, which is colored as bright red (in Figure 5(i)) at top right). This county is influenced in the previous cut-point and has now been severely affected (after October 4), and the influence has spread to nearby counties as well.

Cut-point 4 (Figure 5(f)) was captured when power outages of the counties started to abate. The explanation results in Figure 5(j) show the important counties whose outages started to decrease at this cut-point.

In addition, interestingly, although both hurricanes Irma and Matthew have similar geographical trajectories, CnR-UV learns very different spatial clusters, which captures counties with variable dynamics (Figure 5(b)).

5.3.4   Details of Baseline Algorithms on Hurricane Data. In contrast to the CnR-UV performance, the baseline algorithms all consistently either fail to converge or under-segment, giving low quality unexplainable cut-points. *TICC* and *AutoPlait* under-segment on some and fail to converge in the case of other hurricane datasets, whereas *DynaMMo* yields over-segmented results. *Floss*, although avoiding convergence and over-segmentation problems, yields segments that only capture the initial rise and final fall of the time series in the case of all of the hurricanes, completely missing out on phases of power failure in between.

5.4 Comparison with CnR-V

We characterized the performance of CnR-V on hurricanes Harvey, Irma, and Matthew power outage data, where there are long-range spatial dependencies, and found that CnR-V gives lower quality cut-points and explanations as expected. As an example, see Figure 4(e) and (i): although CnR-V is able to capture this cut-point (Figure 6(d) and (g)), its explanations only point to the sudden rise in a small cluster of spatially close counties; it fails to capture the large decrease in Nueces County (cyan line) (which CnR-UV is able to) because Nueces is not geographically close to the other ones.
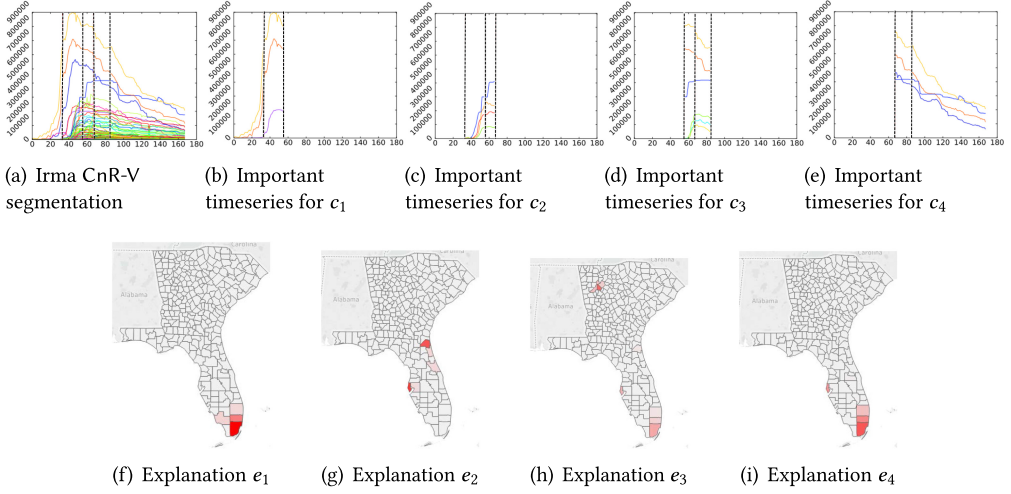
(a) Irma CnR-V
segmentation

(b) Important
timeseries for c_1

(c) Important
timeseries for c_2

(d) Important
timeseries for c_3

(e) Important
timeseries for c_4

(f) Explanation e_1 (g) Explanation e_2 (h) Explanation e_3 (i) Explanation e_4

Fig. 7. Segmentations and explanations results of CnR-V for Hurricane Irma analogous to Figure 3.

5.4.1 Comparison Results of Hurricane Harvey. Cut-point 1 (Figure 4(c)) is only captured by CnR-UV and not captured by CnR-V. In this cut-point, El Paso, Howard, and other counties in central Texas were considered important in Figure 4(g) because they were flood affected due to Hurricane Harvey. Cut-point 2 (Figure 4(d)) captured by CnR-UV is similar to the first cut-point of Figure 6(b) captured by CnR-V. However, some counties (Fort Bend, Harris, and Brazoria) are also considered important (from reports, it was found that some major damage occurred in those spots due to a tornado; see details in Section 5.3.2) by CnR-UV but not captured by CnR-V. Cut-point 3 (Figure 4(e)) by CnR-UV is similar to the cut-point depicted in Figure 6(c) discovered by CnR-V. Montgomery (orange line) is also considered as an important county in CnR-V but not highlighted in Figure 4(e) by CnR-UV. Upon further investigation, we found that this county did not face any major damage around this time, but it was shown to be important by CnR-V only because it is geographically close to Harris. Cut-point 4 (Figure 4(f)) discovered by CnR-UV is similar to the cut-point depicted in Figure 6(d) discovered by the CnR-V model. However, Figure 6(d) does not capture Nueces (green line), which has a high decrease of outage. Hence, CnR-V only captures increase of outages at this cut-point, whereas CnR-UV captures both increasing and decreasing trends simultaneously.

5.4.2 Comparison Results of Hurricane Irma. For better understanding, the figures for CnR-V are shown in Figure 7 for segmentation and explanation. CnR-V could not capture the small rising trend in Figure 3(d) and fluctuation of outages in Figure 3(e) separately as CnR-UV. CnR-V only identifed a cut-point near 50 (Figure 7(c)), which did not explain the counties that had fluctuation of outages (see Section 5.3.1 for a detailed description). Moreover, if we compare the geographical explanation of counties of CnR-V in Figure 7(f) through (i) with CnR-UV in Figure 3(h) through (l), we observe that CnR-V could not capture the long-range spatial dependencies of counties, and they were sparse.

5.4.3 Comparison Results of Hurricane Matthew. We were unable to run the entire Matthew dataset on CnR-V and hence considered a sub-sampled version to obtain cut-points using CnR-V. We notice that CnR-V is unable to capture cut-point 1 (Figure 5), where it fails to capture a few important counties (Figure 5(g)) on the southern tip of Florida that are captured by CnR-UV. It must be noted that in the case of each hurricane, there is no notion of spatial clustering in the

Table 4. Scalability Experiment Varying the
Number of Time Series Keeping Timesteps
Constant at 720

No. of Time Series	CnR-V	CnR-UV
15	734.37	179.07
30	733.39	180.35
60	822.99	173.44
120	835.65	184.50
240	863.03	190.47
480	952.81	210.45

(Wall clock time seconds).

Table 5. Scalability Experiment Varying the
Number of Timesteps Keeping Time Series
Constant at 15

No. of Timesteps	CnR-V	CnR-UV
500	285.19	64.63
1,500	7,388.49	115.38
2,500	25,755.02	3,660.25

(Wall clock time seconds).

case of CnR-V, and spatial clusters similar to those represented in Figures 3(b), 4(b), and 5(b) are obtained only by CnR-UV.

5.4.4 Scalability Comparison. We also recorded the runtimes (in seconds) for CnR-V and CnR-UV after varying both the number of timesteps and time series in the dataset. We get better scaling in practice (from our worst-case complexities): in both cases, CnR-UV (due to the low-dimensional latent factor representation) scales quadratically, whereas CnR-V is significantly more expensive (sub-cubic in the number of timesteps). We performed two kinds of experiments, one wherein the number of timesteps in the dataset was maintained constant (720 timesteps) while the number of time series were varied (Table 4), and the other where we maintained the number of time series constant (15 time series) and the number of timesteps were varied (Table 5). The results indicate that in both cases, CnR-UV is more scalable with increasing numbers of time series and increasing numbers of timesteps. This can be attributed to our choice of representing U and V in Equation (5) as low-dimensional latent factor weight matrices instead of full square matrices where $U \in \mathbb{R}^{n \times n}$ and $V \in \mathbb{R}^{m \times m}$ as in the case of CnR-V. We also include scalability comparisons of CnR-UV with other state-of-the-art baselines in the appendix [6]. In these comparisons, we noticed that CnR-UV scaled equally as well as the *Floss* model and better than the *TICC* and *DynaMMo* models with increasing numbers of time series. CnR-UV scales quadratically in the number of timesteps; future work will be aimed at caching and smart computational strategies to scale it to larger datasets.

5.5 Summary of Observations

(1) CnR-UV consistently outperforms the baseline algorithms (up to *0.79x*) in all datasets (including with ground truth) for both time series segmentations and explanations (for hurricanes, the baselines heavily under-segment or do not even finish).

(2) For hurricane datasets, CnR-UV discovers non-trivial cut-points capturing the overall trajectory, as well as subtle anomalies like a combination of sudden increasing and/or decreasing clusters of outage trends and plateaus across regions. CnR-UV also discovers useful spatial clusters of counties based on their location and outages.

(3) Most importantly, we are also able to identify an informative set of culprit time series for each cut-point, providing valuable insights to the domain experts aiding management, recovery, and resource allocation efforts.

(4) CnR-UV scales quadratically with the number of timesteps as opposed to CnR-V, which scales sub-cubically.

6 RELATED WORK

We will now review lines of research that have attempted to answer questions similar to our goals in this article.

Time series segmentation. There has been an abundance of work on time series segmentation based on monitoring changing temporal patterns, such as modeling co-evolving time series and segmenting them using multi-level HMMs [35] on motion capture data, discovering patterns in data streams [46] using distributed video data, developing online algorithms for frequent sequence mining [36] on different application domains (i.e., robotics, wild life, and health monitoring), and time series segmentation using a temporal mixture model and Bayesian information criterion on railway data [48] and Kalman filters on motion capture sequences and chlorine measurement data [32]. GOALIE [42] is another algorithm applied in the context of biological process data that produces segmentations of multivariate time series, but its focus is on finding cut-points where significant shifts of clusters (of time series) occur, in contrast to CnR-UV wherein the focus is both on recovering the major segments and explaining the segments while leveraging the underlying spatial structure of the data.

Change point detection has also been a popular topic in the climate sciences [43, 49]. Characterizing the dynamics of natural disasters like hurricanes lends itself naturally to a change point detection approach, but there has been little work conducted in this regard. Zhao and Chu [58] propose a hierarchical Bayesian framework for detecting shifts in annual hurricane counts, whereas Ruggieri [47] introduces a Bayesian change point detection algorithm to detect changes in temperature using climate data records. The other line of work on modeling failure cascading on CIS [18] does not explicitly segment the time series. Despite the extensive research conducted in time series segmentation and change point detection, we have found that little prior work exists in leveraging them to characterize the dynamic effect natural disasters have on CIS.

Two limitations of previous work in temporal segmentation are that not many of them easily incorporate spatial information into temporal segmentation, and none of the existing models provide any explanation framework wherein "culprit" counties (at each segment of a hurricane failure process) can be identified in space *and* time. Most change point work is focused only on identifying temporal cut-points [9] with a few applications in computer vision and video analysis modeling spatial relationships [14, 51], but no work has identified important time series (i.e., spatial) thereby providing an explanation of each identified temporal segment. Such a model that identifies "culprit" counties is helpful to experts involved in maintenance of cyber-physical infrastructure and teams responsible for disaster management and planning.

Another line of related work in time series corresponds to subspace clustering–based techniques. Many applications in multivariate time series analysis exist wherein the temporal data is drawn from multiple spaces and hence exhibits multi-segment behavior. It is often useful to develop techniques to represent the data in a subspace to capture richer temporal relationships and apply clustering to explicitly demarcate these multiple segments. This approach called *subspace clustering* has been applied to video and image segmentation [33, 52, 55], image compression [29], and spatio-temporal action segmentation [20, 31]. A comprehensive review about the different types of subspace clustering methods is provided by Vidal [53]. There has been extensive work in subspace clustering in data mining [40], but to the best of our knowledge, it has not been applied on hurricane outage data for finding the temporal relation among timesteps. Further, these subspace clustering techniques do not provide explanations of the results.

Simple interpretable models. There has recently been a push toward quantifying model uncertainty [22] and making machine learning model outputs quantifiable, explainable, and simple [45]. Poursabzi-Sangdeh et al. [41] presented literature where they designed several quantitative and qualitative experiments to investigate the impact of features and model transparency on model prediction, a measure of trust and explainability. These models and their explanations are specific to the underlying machine learning models and cannot be applied to our segmentation problem. We

find that temporal segmentation is inherently unsupervised, and the intuition behind the segments might not be readily apparent or explainable in certain applications. To the best of our knowledge, our explanation optimization problem is the first attempt at designing simple explanations for time series segments. In such cases, producing interpretable, simple segmentation results are effective in addressing the explainability problem.

Spatio-temporal models. Yao et al. [56] developed the spatio-temporal dynamic network (STDN) for traffic flow prediction. Our CnR-UV model is designed to recover explainable segments of the major failure phases in data containing bursty time series that do not contain periodic, cyclical effects like traffic flow patterns. Wu et al. [54] propose an urban anomaly prediction (UAPD) model with a change point detection facet to detect evolving anomaly patterns. In contrast, CnR-UV, in addition to detecting the major change points (i.e., segments) of the data, is able to return sparse explanations about each retrieved change point yielding a holistic representation of the change point.

In this article, we propose a dual-objective segmentation framework designed to provide spatio-temporal segments of the data and simple explanations of the generated segments. Our proposed framework optimizes the segmentation and explanation to obtain simple interpretable and sparse segmentations of the data. We demonstrate our model on the dynamic degradation of critical infrastructure during natural calamities. To the best of our knowledge, this is the first attempt toward designing simple explainable segments of time series data.

7 CONCLUSION

In this work, we developed a novel effective and scalable combined framework CnR for providing segmentations and simple interpretable explanations for multivariate time series like outage data. We evaluated the performance of our methodology against state-of-the-art segmentation and time series clustering procedures on open ground-truth datasets. We also conducted an extensive analysis on the failure of the power grid during three hurricane events. There are many avenues for future work. Methodologically, we can explore performing a joint learning of segmentations and explanations, and more complex explanations. We can also explore integrating CnR with existing analysis tools, such as the URBANNET toolkit [18] in use in national laboratories.

REFERENCES

[1] Boston Herald. 2017. Hurricane Harvey. Retrieved June 16, 2020 from https://www.bostonherald.com/2017/08/25/hurricane-harvey-to-slam-texas-coast-hard/.

[2] Carnegie Mellon University. 2014. CMU Graphics Lab Motion Capture Database. Retrieved June 16, 2020 from http://mocap.cs.cmu.edu.

[3] Dekalb County Georgia. 2017. Georgia Power Working to Restore Service to 161,000 in DeKalb. Retrieved June 16, 2020 from https://www.dekalbcountyga.gov/news/georgia-power-working-restore-service-161000-dekalb.

[4] 2017. Major Storm System Impacting Holiday Travel Through Friday. Retrieved June 16, 2020 from https://www.weather.gov/crp/hurricane_harvey.

[5] NOAA's National Weather Service. 2017. Severe Weather Event Review for Saturday August 26 2017. Retrieved June 16, 2020 from http://www.spc.noaa.gov/exper/archive/event.php?date=20170826.

[6] 2019. Appendix. Retrieved June 16, 2020 from https://bit.ly/2JVt8GP.

[7] GitHub. 2020. Code and Datasets. Retrieved June 16, 2020 from https://github.com/anikat1/cnr-tist/blob/master/appendix.pdf.

[8] M. Allen, S. Fernandez, O. Omitaomu, and K. Walker. 2014. Application of hybrid geo-spatially granular fragility curves to improve power outage predictions. *Journal of Geography & Natural Disasters* 4, 127 (2014), 2167–0587.

[9] Samaneh Aminikhanghahi and Diane J. Cook. 2017. A survey of methods for time series change point detection. *Knowledge and Information Systems* 51, 2 (2017), 339–367.

[10] Francis Bach, Rodolphe Jenatton, Julien Mairal, and Guillaume Obozinski. 2011. Convex optimization with sparsity-inducing norms. *Optimization for Machine Learning* 5 (2011), 19–53.

[11] Oresti Banos, Mate Attila Toth, Miguel Damas, Hector Pomares, and Ignacio Rojas. 2014. Dealing with the effects of sensor displacement in wearable activity recognition. *Sensors* 14, 6 (2014), 9995–10023.

[12] Alan M. Barker, Eva B. Freer, Olufemi A. Omitaomu, Steven J. Fernandez, Supriya Chinthavali, and Jeffrey B. Kodysh. 2013. Automating natural disaster impact analysis: An open resource to visually estimate a hurricane's impact on the electric grid. In *Proceedings of the IEEE Southeast Conference*. IEEE, Los Alamitos, CA, 1–3.

[13] Richard H. Bartels and George W. Stewart. 1972. Solution of the matrix equation AX + XB = C [F4]. *Communications of the ACM* 15, 9 (1972), 820–826.

[14] Durell Bouchard. 2006. *Automated Time Series Segmentation for Human Motion Analysis. Center for Human Modeling and Simulation, University of Pennsylvania.*

[15] Stephen Boyd, Neal Parikh, Eric Chu, Borja Peleato, and Jonathan Eckstein. 2011. Distributed optimization and statistical learning via the alternating direction method of multipliers. *Foundations and Trends® in Machine Learning* 3, 1 (2011), 1–122.

[16] Liang Chang and Zhigang Wu. 2011. Performance and reliability of electrical power grids under cascading failures. *International Journal of Electrical Power & Energy Systems* 33, 8 (2011), 1410–1419.

[17] Liangzhe Chen, Sorour E. Amiri, and B. Aditya Prakash. 2018. *Automatic Segmentation of Data Sequences*. Association for the Advancement of Artificial Intelligence.

[18] Liangzhe Chen, Xinfeng Xu, Sangkeun Lee, Sisi Duan, Alfonso G. Tarditi, Supriya Chinthavali, and B. Aditya Prakash. 2017. HotSpots: Failure cascades on heterogeneous critical infrastructure networks. In *Proceedings of the 2017 ACM Conference on Information and Knowledge Management (CIKM'17)*. ACM, New York, NY, 1599–1607.

[19] Eagle. 2012. Eagle-I. Retrieved June 16, 2020 from https://eagle-i.doe.gov/.

[20] Ehsan Elhamifar and René Vidal. 2009. Sparse subspace clustering. In *Proceedings of the 2009 IEEE Conference on Computer Vision and Pattern Recognition (CVPR'09)*. IEEE, Los Alamitos, CA, 2790–2797.

[21] Rozhin Eskandarpour and Amin Khodaei. 2017. Machine learning based power grid outage prediction in response to extreme events. *IEEE Transactions on Power Systems* 32, 4 (2017), 3315–3316.

[22] Zoubin Ghahramani. 2015. Probabilistic machine learning and artificial intelligence. *Nature* 521, 7553 (2015), 452.

[23] Shaghayegh Gharghabi, Yifei Ding, Chin-Chia Michael Yeh, Kaveh Kamgar, Liudmila Ulanova, and Eamonn Keogh. 2017. Matrix profile VIII: Domain agnostic online semantic segmentation at superhuman performance levels. In *Proceedings of the 2017 IEEE International Conference on Data Mining (ICDM'17)*. IEEE, Los Alamitos, CA, 117–126.

[24] Gene Golub, Stephen Nash, and Charles Van Loan. 1979. A Hessenberg-Schur method for the problem AX + XB = C. *IEEE Transactions on Automatic Control* 24, 6 (1979), 909–913.

[25] David Hallac, Sagar Vare, Stephen Boyd, and Jure Leskovec. 2017. Toeplitz inverse covariance-based clustering of multivariate time series data. In *Proceedings of the 23rd ACM SIGKDD International Conference on Knowledge Discovery and Data Mining (KDD'17)*. ACM, New York, NY, 215–223.

[26] Paul Hines, Karthikeyan Balasubramaniam, and Eduardo Cotilla Sanchez. 2009. Cascading failures in power grids. *IEEE Potentials* 28, 5 (2009), 24–30.

[27] Paul D. H. Hines, Ian Dobson, and Pooya Rezaei. 2017. Cascading power outages propagate locally in an influence graph that is not the actual grid topology. *IEEE Transactions on Power Systems* 32, 2 (2017), 958–967.

[28] Åke J. Holmgren. 2006. Using graph models to analyze the vulnerability of electric power networks. *Risk Analysis* 26, 4 (2006), 955–969.

[29] Wei Hong, John Wright, Kun Huang, and Yi Ma. 2006. Multiscale hybrid linear models for lossy image representation. *IEEE Transactions on Image Processing* 15, 12 (2006), 3655–3671.

[30] Yehuda Koren, Robert Bell, and Chris Volinsky. 2009. Matrix factorization techniques for recommender systems. *Computer* 42, 8 (2009), 30–37.

[31] Colin Lea, Austin Reiter, René Vidal, and Gregory D. Hager. 2016. Segmental spatiotemporal CNNs for fine-grained action segmentation. In *Proceedings of the European Conference on Computer Vision (ECCV'16)*. 36–52.

[32] Lei Li, James McCann, Nancy S. Pollard, and Christos Faloutsos. 2009. DynaMMo: Mining and summarization of coevolving sequences with missing values. In *Proceedings of the 15th ACM SIGKDD International Conference on Knowledge Discovery and Data Mining (KDD'09)*. ACM, New York, NY, 507–516.

[33] Junmin Liu, Yijun Chen, Jiangshe Zhang, and Zongben Xu. 2014. Enhancing low-rank subspace clustering by manifold regularization. *IEEE Transactions on Image Processing* 23, 9 (2014), 4022–4030.

[34] Jun Liu and Jieping Ye. 2010. Efficient l1/lq norm regularization. arXiv:1009.4766.

[35] Yasuko Matsubara, Yasushi Sakurai, and Christos Faloutsos. 2014. AutoPlait: Automatic mining of co-evolving time sequences. In *Proceedings of the 2014 ACM SIGMOD International Conference on Management of Data (SIGMOD'14)*. ACM, New York, NY, 193–204.

[36] Abdullah Mueen and Eamonn Keogh. 2010. Online discovery and maintenance of time series motifs. In *Proceedings of the 16th ACM SIGKDD International Conference on Knowledge Discovery and Data Mining (KDD'10)*. 1089–1098.

[37] Nikhil Muralidhar, Chen Wang, Nathan Self, Marjan Momtazpour, Kiyoshi Nakayama, Ratnesh Sharma, and Naren Ramakrishnan. 2018. illiad: InteLLigent invariant and anomaly detection in cyber-physical systems. *ACM Transactions on Intelligent Systems and Technology* 9, 3 (2018), 35.

[38] Xia Ning and George Karypis. 2011. SLIM: Sparse linear methods for top-n recommender systems. In *Proceedings of the 2011 IEEE 11th International Conference on Data Mining (ICDM'11)*. IEEE, Los Alamitos, CA, 497–506.

[39] Min Ouyang. 2014. Review on modeling and simulation of interdependent critical infrastructure systems. *Reliability Engineering & System Safety* 121 (2014), 43–60.

[40] Lance Parsons, Ehtesham Haque, and Huan Liu. 2004. Subspace clustering for high dimensional data: A review. *ACM SIGKDD Explorations Newsletter* 6, 1 (2004), 90–105.

[41] Forough Poursabzi-Sangdeh, Daniel G. Goldstein, Jake M. Hofman, Jennifer Wortman Vaughan, and Hanna Wallach. 2018. Manipulating and measuring model interpretability. arXiv:1802.07810.

[42] Naren Ramakrishnan, Satish Tadepalli, Layne T. Watson, Richard F. Helm, Marco Antoniotti, and Bud Mishra. 2010. Reverse engineering dynamic temporal models of biological processes and their relationships. *Proceedings of the National Academy of Sciences* 107, 28 (2010), 12511–12516.

[43] Jaxk Reeves, Jien Chen, Xiaolan L. Wang, Robert Lund, and Qi Qi Lu. 2007. A review and comparison of changepoint detection techniques for climate data. *Journal of Applied Meteorology and Climatology* 46, 6 (2007), 900–915.

[44] Andreas Reinhardt, Paul Baumann, Daniel Burgstahler, Matthias Hollick, Hristo Chonov, Marc Werner, and Ralf Steinmetz. 2012. On the accuracy of appliance identification based on distributed load metering data. In *Proceedings of the 2012 Conference on Sustainable Internet and ICT for Sustainability (SustainIT'12)*. IEEE, Los Alamitos, CA, 1–9.

[45] Marco Tulio Ribeiro, Sameer Singh, and Carlos Guestrin. 2016. "Why should I trust you?": Explaining the predictions of any classifier. In *Proceedings of the 22nd ACM SIGKDD International Conference on Knowledge Discovery and Data Mining (KDD'16)*. ACM, New York, NY, 1135–1144.

[46] Guy Rosman, Mikhail Volkov, Dan Feldman, John W. Fisher III, and Daniela Rus. 2014. Coresets for *k*-segmentation of streaming data. In *Proceedings of the 27th International Conference on Neural Information Processing Systems—Volume 1 (NIPS'14)*. 559–567.

[47] Eric Ruggieri. 2013. A Bayesian approach to detecting change points in climatic records. *International Journal of Climatology* 33, 2 (2013), 520–528.

[48] Allou Samé and Gérard Govaert. 2012. Online time series segmentation using temporal mixture models and Bayesian model selection. In *Proceedings of the 2012 11th International Conference on Machine Learning and Applications (ICMLA'12)*. 602–605.

[49] Rishu Saxena, Layne T. Watson, Randolph H. Wynne, Evan B. Brooks, Valerie A. Thomas, Yang Zhiqiang, and Robert E. Kennedy. 2018. Towards a polyalgorithm for land use change detection. *ISPRS Journal of Photogrammetry and Remote Sensing* 144 (2018), 217–234.

[50] Jianbo Shi and Jitendra Malik. 2000. Normalized cuts and image segmentation. *IEEE Transactions on Pattern Analysis and Machine Intelligence* 22, 8 (2000), 888–905.

[51] Yuliya Tarabalka, Guillaume Charpiat, Ludovic Brucker, and Bjoern H. Menze. 2014. Spatio-temporal video segmentation with shape growth or shrinkage constraint. *IEEE Transactions on Image Processing* 23, 9 (2014), 3829–3840.

[52] Stephen Tierney, Junbin Gao, and Yi Guo. 2014. Subspace clustering for sequential data. In *Proceedings of the IEEE Conference on Computer Vision and Pattern Recognition (CVPR'14)*. 1019–1026.

[53] René Vidal. 2011. Subspace clustering. *IEEE Signal Processing Magazine* 28, 2 (2011), 52–68.

[54] Xian Wu, Yuxiao Dong, Chao Huang, Jian Xu, Dong Wang, and Nitesh V. Chawla. 2017. UAPD: Predicting urban anomalies from spatial-temporal data. In *Proceedings of the Joint European Conference on Machine Learning and Knowledge Discovery in Databases*. 622–638.

[55] Allen Y. Yang, John Wright, Yi Ma, and S. Shankar Sastry. 2008. Unsupervised segmentation of natural images via lossy data compression. *Computer Vision and Image Understanding* 110, 2 (2008), 212–225.

[56] Huaxiu Yao, Xianfeng Tang, Hua Wei, Guanjie Zheng, and Zhenhui Li. 2019. Revisiting spatial-temporal similarity: A deep learning framework for traffic prediction. In *Proceedings of the AAAI Conference on Artificial Intelligence*, Vol. 33. 5668–5675.

[57] Yinyu Ye and Edison Tse. 1989. An extension of Karmarkar's projective algorithm for convex quadratic programming. *Mathematical Programming* 44, 1–3 (1989), 157–179.

[58] Xin Zhao and Pao-Shin Chu. 2006. Bayesian multiple changepoint analysis of hurricane activity in the eastern North Pacific: A Markov chain Monte Carlo approach. *Journal of Climate* 19, 4 (2006), 564–578.